Journal of
Materials Chemistry B

Accepted Manuscript

This article can be cited before page numbers have been issued, to do this please use: S. K. Tuteja, T. Duffield and S. Neethirajan, *J. Mater. Chem. B*, 2017, DOI: 10.1039/C7TB01382E.

ROYAL SOCIETY OF CHEMISTRY

rsc.li/materials-b

View Article Online
DOI: 10.1039/C7TB01382E

Graphene based Multiplexed disposable electrochemical biosensor for on-farm rapid monitoring of NEFA and βHBA Dairy biomarkers

Satish K. Tuteja[1], Todd Duffield[2], Suresh Neethirajan[1]*

[1]BioNano Laboratory, School of Engineering, University of Guelph, Guelph, ON, N1G 2W1, Canada

[2]Todd Duffield, Population Medicine, Ontario Veterinary College, University of Guelph, Guelph, ON, N1G 2W1, Canada

*Corresponding author:

E-mail address: sneethir@uoguelph.ca (S. Neethirajan).

View Article Online
DOI: 10.1039/C7TB01382E

Abstract

Elevated circulating concentrations of non-esterified fatty acids (NEFA) and Beta hydroxy butyrate (βHBA) in biological fluids are recognized as critical biomarkers for early diagnosis of Negative Energy Balance (NEB) in dairy cow. Herein, we report the development of a cost-effective, bio-friendly and electrochemically active dual screen printed electrode (SPE) sensor platform composed of Electro reduced Graphene oxide nanosheets (E-rGO) modified with specific antibodies against the NEFA and βHBA. The chemically synthesized graphene oxide (GO) was reduced directly on the screen printed electrode (SPE) surface via green electrochemical approach without using toxic chemicals. The E-rGO was characterized using various analytical techniques like XPS, SEM, TEM, AFM, UV-Vis, Raman spectroscopy, FTIR, and XRD, to get insight to its properties. Electrochemical analysis demonstrates that the E-rGO modified SPEs electrodes exhibit enhanced and durable redox properties as compared to the pristine graphite and GO electrodes. Targets specificity is accomplished through immobilization of specific antibodies against NEFA and βHBA over the surface of nanostructure immobilized SPE, which only interacts with its counterpart NEFA and βHBA only. The antibodies retain their characteristic of immuno-complex formation property upon immobilization and exhibit changes to amperometric signals upon interaction with various concentrations of NEFA and βHBA in standard, spiked blood and real clinical samples. The DPV signals resulted from the developed immunosensor platform exhibited a good correlation ($R^2 \sim 0.99$ for both NEFA and βHBA) for the wide range of target concentrations from 0.1 mM to 10 mM. The proposed immunosensor design not only provides rapid analytical response time (≥1 min), but simplicity in fabrication and instrumentation, which may provide a promising approach for on-farm diagnostics of ketosis and metabolic disorders associated with NEB.

View Article Online
DOI: 10.1039/C7TB01382E

Keywords: NEFA; Graphene; βHBA; Ketosis; On-farm biosensor

1. Introduction

Now a days, Carbon (Graphite, Graphene, CNTs) based screen printed electrodes (SPEs) are very fascinating and efficient material for biosensor applications due to easy to operate, simple function, economical, disposable and can be employed for hand-held diagnostic, on-farming and POC (point-of-care) monitoring[1]. Amongst the carbon SPEs, 2-Dimensional Graphene nanostructures based potential redox active surface are the novel nanomaterials and receiving much attention in the diagnostic device construction[2], due to versatile biocompatibility to biological molecules, economical bulk preparation and enhanced electron amplification[3]. Graphene is a 2-dimensional honeycomb lattice structure of single atomic sheet of carbon with sp^2 hybridisation. At present on this planet, Graphene is well known for its highly conducting nature and electronics properties[4,5]. During last decade, graphene has become a novel nanomaterial for the research due to its intriguing characteristics, such as quantum electron transport[6,7], tunable band gap[8], high carrier mobility[9], high elastic behavior[10], and excellent electrochemical properties[11–13]. In recent years, due to commercialization and advancement in the synthesis processes of Graphene becomes successful in the various field of applications like semiconductor industry, electronics, batteries, supercapacitor, fuel cells, chemical industry and biosensing technology[14–16].

Due to ease of surface modification characteristics and high charge mobility, Graphene has been successfully anticipated as a promising material for the realization of highly sensitive, high performance biosensor[5,17,18] for numerous sensing applications[19–21]. The property of bonding of the hexagonal region of graphene with other aromatic molecules through π–π aromatization based supra molecular interaction, and ease of chemical functionalization provide escalated

View Article Online
DOI: 10.1039/C7TB01382E

performance of the associated bio-detection devices[22,23]. The facile Graphene functionalization processes helps to become dispersible in various solvents and buffers. The pristine Graphene has negligible functional groups on its surface, however, for the biosensing applications graphene should be functionalized with suitable functional groups to conjugate with proteins, antibodies etc.[24]. For this purpose various approaches of functionalization has been used like carboxylation, polymerization, amidation and decoration with nanoparticles for the nanocomposite formation. The Graphene oxide (GO) is the oxidized and less conducting form of the Graphene and has abundant carboxyl, hydroxyl and epoxyl etc. chemical moieties on its surface. The hydroxyl and epoxyl groups are mainly responsible for the non-conduction behavior of Graphene sheets, to make electroconducting GO must be reduced.

Among the various determined and optimized chemical method for the reduction of graphene or the synthesis of rGO (reduced graphene oxide), researchers are now paying attention towards electrochemical reduction of GO to form rGO[25,26]. The electrochemical-based reduction is the green route to remove the hydroxyl and epoxyl groups from the graphene oxide to convert it in to rGO with the intact carboxyl groups. Thus, the rGO can be defined as a derivative of graphene that has been partially reduced. The carboxyl groups likely to be present on its surface act as binding sites for chemical sensing and can be further employed for the bioconjugation of proteins by carbodiimide covalent chemistry means using EDS-NHS linkers. This particular feature is of an additional benefit, as it can help to avoid the need for pretreating sensor surfaces with additional chemical linkers such as APTES (3-aminoproplytriethoysilane). Other alternative routes such as thiolation, silanization, carboxylation with mercaptopropionic acid, *in situ* reduction of metal ions, ring-opening polymerization, esterification, free radical polymerization and disulfide linkage, invariably require tedious processing steps. The electrochemical approach

View Article Online
DOI: 10.1039/C7TB01382E

offers a more controllable and effective way for the reduction of oxygen functionalities by simply adjusting the electrode potentials without using hazardous chemicals and chemically reducing. Whilst, the chemical approach may require more than one reducing agents or steps to achieve effective reduction of oxygen functionalities of the GO to the same extent. Moreover, the resulting graphene also tend to agglomerate upon reduction in the liquid phase. Conversely, electrochemical approach may produce graphene directly onto the electrode substrates, which could be used for specific applications, such as biosensor development and electrocatalysis without further steps or treatments. This method offers several advantages over other graphene fabrication techniques, including being green, efficient, inexpensive, and rapid. More importantly, the E-rGO could form a stable film on the electrode surface without any further treatment. The antigen or analyte binding events at the interface between Graphene and charged biomolecules can be directly interpreted through various electrochemical parameters such as resistance, threshold voltage, electron mobility and conductance, etc.

In the present report, Graphene nanosheets were electroreduced and electrodeposited on the dual working area of SPE, for the fast, label-free, electrochemical immunosensing of β-hydroxybutyrate (βHBA) and Non esterified fatty acid (NEFA) biomarkers of cattle. The elevated circulating concentration level of βHBA and NEFA are associated with the negative energy balance of cows and are recognized as critical biomarkers for early diagnosis of dairy cow metabolic diseases. Negative Energy Balance (NEB) in a dairy cattle caused by the increased energy demands at periparturient period is a serious illness that significantly affects the livestock production[27,28]. The critical threshold/cutoff concentration of βHBA is 1.2 mM which is used to differentiate between healthy cattle and cattle with Sub Clinical Ketosis (SCK). The

View Article Online
DOI: 10.1039/C7TB01382E

fluctuation of βHBA concentration in blood from 1.2 to 2.9 mM is considered indicative of SCK[29–31]. The critical threshold blood NEFA concentrations at pre-partum and post-partum are ≥0.3 and ≥0.6 mM, respectively[31,32]. Therefore, regular and early stage monitoring of βHBA and NEFA is clinically important for the dairy cow's health management, and to prevent the onset of clinical disease. Monitoring SCK at an early stage in the disease can help to minimize the economic losses on a dairy and stress induced in animals.

Due to lack of on-farm diagnostic tests for NEB, blood samples from dairy cows are collected and sent to the off-site laboratories for further testing and assessments. Conventional methods (such as ELISA, HPLC, GC-MS, LC-MS and enzymatic colorimetry) are expensive, time consuming, requires trained personnel and rely on large laboratory equipment. As a result, the accessibility of such techniques remains limited and they cannot be used for on-farm monitoring[33]. Therefore there is an urgent need for a facile, sensitive and selective on-farm detection system to facilitate quick decision making regarding negative metabolism and for the regular monitoring of SCK and NEB in dairy cows. Electrochemical-based sensors have been shown to be advantageous for on-farm monitoring[28]. Amongst the various classes of biosensors (*e.g.* electrochemical, bioluminescent, resonant mirror, opto-electric, thermistor, *etc.*), electrochemical biosensors are an attractive choice due to the direct conversion of a biological event into an electronic read-out signal. An electrochemical biosensor essentially consists of a transduction platform immobilized with specific bioreceptor(s) to attain the desired sensitivity and specificity. In this report, antibody immobilized E-rGO is playing an active role of biorecognition layer as well as transducing platform. In this research, our aim was to devise an

View Article Online
DOI: 10.1039/C7TB01382E

immunosensor for the highly sensitive and simultaneous detection of βHBA and NEFA from single drop of blood and results can be interpreted at the cow side.

Herein, we report the successful fabrication of Graphene nanostructures immobilized on dual working SPEs, which are further conjugated with βHBA and NEFA antibodies, for the label-free electrochemical detection of the βHBA and NEFA antigen. The Graphene nanostructures act as a synergistic transducing template for the signal amplification as well as the biointerface for the facile immobilization of antibodies on their 2-dimensional surface with simple bioconjugation chemistry. We carried out the exfoliation by sonication and electrodeposition of highly conducting graphene nanostructures followed by electroreduction and their conjugation with a specific antibody for βHBA and NEFA on the 2D surface of electro reduced graphene (E-rGO). The whole assay is label-free without the use of any enzymes or other labeling agents. A schematic representation of this proposed approach is illustrated in figure 1, which has been shown to be a robust, site-directed, antibody-based biointerface for the detection of the βHBA and NEFA antigen. To the best of our knowledge, till date, there is presently no single one antibody and electrochemical-based assay hand held device method reported for the simultaneous on-farm detection of NEFA and βHBA analysis of cattle for NEB and SCK diagnosis. Herein, we demonstrate for the first time a label-free, electrochemical-based immunosensor for the simultaneous accurate sensing of βHBA and NEFA using a low volume of standard antigen solutions, spiked blood as well as real clinical samples (~50 µL). The advantage of which is fast reaction, minimal usage of toxic chemicals and direct deposition of nanostructures on electrode surface. Therefore, the resulting material do not get contaminated[34]. The obtained results are also validated with a commercial βHBA and NEFA colorimetric kit and a central laboratory based chemical analyzer technique. The proposed approach has the

View Article Online
DOI: 10.1039/C7TB01382E

advantages of being simple and rapid (<1 min) for on-farm detection of NEB by monitoring the concentration of βHBA and NEFA by virtue of biomolecular interactions at the 2-dimensional Graphene nanostructures immobilized dual working electrode surface.

2. Experimental section

2.1. Materials

βHBA antibodies, NEFA antibodies and NEFA colorimetric kit were purchased from Mybiosource, USA. The βHBA colorimetric assay kit was purchased from Cayman Chemical, USA. Graphene Oxide, D(+) glucose (Glu), L-ascorbic acid (AA), uric acid (UA) and lactic acid solution (LA), Oleic acid, potassium hexacyanoferrite ($K_3[Fe(CN)_6]$), potassium hexacyanoferrate ($K_4[Fe(CN)_6]$), β-hydroxybutyric acid, BSA (Bovine Serum Albumin), N-Hydroxysuccinimide (NHS), N-(3-Dimethylaminopropyl)-N′-ethylcarbodiimide hydrochloride (EDC) and phosphate-buffered saline (PBS, pH 7.4) were procured from Sigma-Aldrich Canada (Oakville, ON, Canada). Milli-Q water (18.2 MΩ) was used in all experiments. The dual working carbon screen printed electrodes (SPEs) used in this study were made of Dropsens (model C1110, Spain). The working area (4 mm diameter) of these SPEs consisted of carbon-paste material, whereas carbon and Ag/AgCl were used to form the counter and reference electrodes, respectively. Sterile Bovine Blood is obtained from Cedarlane, Canada.

2.2. Characterization

XRD (X-ray diffraction) analysis was performed with a Bruker Eco D8 advance diffractometer using Cu Kα radiation at the scan rate of 1° min^{-1}. Atomic force microscopic (AFM) investigations were carried out in the noncontact mode using an AGILENT AFM/SPM 5500.

View Article Online
DOI: 10.1039/C7TB01382E

Raman spectra were measured using a Renishaw spectrometer (514 nm excitation wavelength, 1.58 eV). All the experiments were carried out at room temperature conditions (RT = 25±2 °C). A transmission electron microscope (TEM- FEI TECHNAI g2f20, 200 keV) and a scanning electron microscope (SEM-FEI Inspect S50, 15V) equipped with an energy dispersive spectrometer (EDS) (Oxford Instruments X-Max 20) were used for the morphological and structural studies. Optical absorbance spectra were measured using a Cary 100 UV-vis spectrophotometer from Agilent Technologies. The surface chemistry of the E-rGO immobilized SPEs were studied by X-ray photoelectron spectroscopic (XPS) analysis using an Omicron XPS spectrometer (operating with an acceleration voltage of 12 kV and a power of 300 W). Measurement of the electrochemical parameters and the subsequent analysis were performed using a μStat400 Biopotentiostat with a 4-electrode connector from DropSens, Spain. Cyclic voltammograms (CVs) were recorded in the −1 to +1 V potential range at a scan rate of 50 mV s^{-1}. The differential pulse voltammetric (DPV) detection was measured in the −1 to +1V potential range at a scan rate of 50 mV s^{-1} with an amplitude of 2 mV and a step potential of 4 mV. Chronoamperometric responses were studied at an applied potential of 0.2 V. Origin Pro 16 (Origin Lab Corporation, MA, USA) was used for the preparation of graphs. A redox probe solution of 10 mM $[Fe(CN)_6]^{3-}$ + 10 mM $[Fe(CN)_6]^{4-}$ was prepared in 100 mM PBS (phosphate buffer saline). Various clinical serum samples from dairy cows, containing a known concentration of βHBA, were provided as a gift from our collaborator, the Animal Health Laboratory, Ontario Veterinary College, University of Guelph. The clinical serum samples with known βHBA concentration were analyzed by using a Roche Cobas 6000 c501 automated chemistry analyzer (Roche Canada, Laval, QC, Canada).

View Article Online
DOI: 10.1039/C7TB01382E

2.3. Graphene Exfoliation, Electroreduction and Electrodeposition

Typically, aqueous brownish GO dispersion containing nanosheets (1 mg/mL) was used for the electrodeposition and further characterization purposes. The GO dispersion was ultasonicated for the physical exfoliation of nanosheets to overcome the Van der Waals forces present between the graphene sheets. Afterwards, 5 µL of exfoliated nanosheets were spread over the working area of SPEs and then 3 reduction scans was given using LSV (Linear sweep voltammetry techniques (at scan rate of 0.1 V/s and step potential of 0.001 V.) in the range of 0 to -1.4 V. After the electroreduction, 10 cycles of CV (recorded in the −1 to +1 V potential range at a scan rate of 50 mV s^{-1}) was used for the electrodeposition of electroreduced GO (E-rGO) and stability curve was obtained. Further, the E-rGO was thoroughly analysed by the spectroscopic and microscopic techniques.

2.4. Antibodies Conjugation and Biointerface development

5 µL of 10 µg mL^{-1} βHBA antibody (stock concentration 200 µg mL^{-1}) and 5 µL of 10 µg mL^{-1} NEFA antibody (stock concentration 4.7 mg mL^{-1}) solution was spread over the E-rGO modified SPEs and incubated for 2 hours at 25 °C. The immobilization of the βHBA and NEFA antibodies on the E-rGO SPEs was carried out *via* EDC-NHS carbodiimide covalent chemistry using EDS-NHS linkers. The protein immobilization on the E-rGO surface was facilitated by covalent chemistry due to the intact –COOH groups present on E-rGO. The surface was then washed with 10 mM PBS solution to remove the unbound antibodies. The electrode surface was then blocked with BSA solution (2 µL, 0.25% w/v) and incubated for 30 min to minimize non-specific protein interactions, before finally being washed with buffer solution. The prepared

View Article Online
DOI: 10.1039/C7TB01382E

immunosensor was then stored at 4 °C when not in use. The successful antibody conjugation on the E-rGO surface was characterized by spectroscopic and electrochemical techniques.

2.5. Label-free electrochemical quantification of βHBA and NEFA antigen

The developed antibody immobilized dual working E-rGO modified Graphene immunosensor was tested for its electrochemical response with respect to varying βHBA and NEFA concentrations. The standard antigen solutions (were prepared in PBS buffer (pH 7.4), spiked bovine blood samples, and real clinical samples containing unknown concentrations of βHBA and NEFA were tested. A small volume (5 µL) of the antigen solution was exposed to the working electrode area of the immunosensor. It was then left to incubate for 15 min at room temperature to ensure the antibody–antigen binding. The incubation time for the efficient binding of antibodies immobilized over SPE with their counter antigen was optimized to get precise results (figure S9, ESI). Then the electrode was washed by gentle immersion in the PBS buffer before analysis of its electrochemical properties with respect to the introduction of a redox probe electrolyte (50 µL of 10 mM $[Fe(CN)_6]^{3-}$ + 10 mM $[Fe(CN)_6]^{4-}$ was prepared in 100 mM PBS). The electrochemical measurements (differential pulse voltammetric and chronoamperometric) were recorded to monitor the change in the current response of the prepared electrodes. Baselines were established by analyzing a blank control sample using PBS buffer only. To further evaluate the practical performance of the electrochemical immunosensor, real serum samples (clinical samples) with unknown concentrations were tested by the electrochemical immunosensor, and the average current response was then calculated to determine the sample concentration. The real serum samples were pretested with a chemical analyzer and provided by AHL, ON, Canada. These provided samples were also analyzed in parallel with detection by a commercial kit

View Article Online
DOI: 10.1039/C7TB01382E

(Cayman Chemicals β-Hydroxybutyrate (Ketone Body) Colorimetric Assay kit, Cedarlane Labs, Burlington, ON, Canada) and NEFA Colorimetric Kit (Mybiosource, USA).

2.6. Cross reactivity, Reproducibility and Storage Stability Studies

The cross reactivity specificity of the developed immunosensor electrodes was evaluated by investigating their response against non-specific interferents, namely L-ascorbic acid (AA), lactic acid solution (LA), uric acid (UA) and D (+) glucose (Glu). The DPV response of the immunosensor surface was recorded after incubating the non-specific analytes. The reproducibility and sensor to sensor variation was also evaluated by repeating the βHBA and NEFA detection experiment, measuring DPV response five times with the same immunosensor and the same concentration of βHBA and NEFA, but with different electrodes (inter and intra assay variations). The stability of the immunosensor was also examined, by carrying out the DPV measurements at different time intervals using the same concentration of βHBA and NEFA, and the immunosensor were stable for 90 days when stored under refrigeration. All the assay experiments conducted at room temperature conditions.

2.7. Real Clinical Samples Studies and Validation

The 4 clinical sample of βHBA and NEFA are also studied with our electrochemical method. The obtained values are tabulated in Table 1 and Table 2 (ESI). The obtained results of the varying concentration of βHBA and NEFA from electrochemical label free immunoassay was compare and validated with Chemical analyzer report as well as traditional colorimetric kit method.

3. Results and discussion

View Article Online
DOI: 10.1039/C7TB01382E

Spectroscopic, structural and morphological features of the E-rGO modified SPE have been assessed instrumentally by the combination of various state of the art techniques. The SEM analysis illustrates the micrograph images of bare dual working Screen printed electrode before electrodeposition (figure 2(a)) and electro deposited graphene modified SPEs (figure 2(b)). The high magnification SEM analysis (shown in figure 2(c) &2(d)) clearly depicts the successful immobilization of graphene nanostructures over the working are of screen printed electrode. The corresponding EDS analysis (figure S10, ESI) highlights the presence of elemental carbon as the major component of the sample. As strong intensity of the observed peak indicates high relative purity of the E-rGO nanosheets.

The electrodeposition over the dual SPEs was further investigated by using AFM and TEM analysis. AFM micrographs and the corresponding height profiling studies illustrates ~ 2 nm in height corresponding to 3-4 graphene layers (figure 2(e)) and corresponding line mapping shown in figure S11 (ESI). For TEM analysis, the deposited material (E-rGO) was carefully separated out from one of the test electrodes. The TEM micrograph of E-rGO are given in figure 2(f) and clearly evident the successful 2D nanosheets deposition over the working area of SPEs. The spectral analysis by FTIR shown in figure 3(a) reveals that the electrochemically converted nanocomposite from GO is left with inadequate major detrimental oxygen functionalities (–OH). It was observed that the characteristic O–H stretching vibrations (oxygen functionalities) at 3400 cm^{-1} found in GO were significantly reduced in E-rGO nanocomposite. However, stretching vibrations from C=O at ~1700 cm^{-1} are still observed in electroreduced nanostructure, while C–O stretching vibrations reflected at 1110 cm^{-1} becomes sharper. This may be attributed due to intact

View Article Online
DOI: 10.1039/C7TB01382E

carboxyl groups after electrochemical reduction. These groups are also responsible for the bioconjugation and hydrophilic nature of the synthesized E-rGO[35–37].

UV–vis studies were carried out to assess the effect of carboxylation and antibody functionalization on the graphene sheets. The UV–vis spectra of GO and E-rGO in solution depicts peaks at 325 nm and 345 nm respectively, attributing to the π- π* transition of aromatic sp^2 domains (figure (3(b)). A red-shift from 325 nm to 345 nm was observed, indicating that there is a less degree of π- π conjugation in GO which is revived with in E-rGO nanocomposite upon electrochemical reduction of (–OH) groups of GO[38]. In the Uv-vis spectra of E-rGO and Antibody bioconjugate (Ab@E-rGO), the appearance of a broad shoulder near 350 nm in the carboxylated graphene sample indicated the success of the chosen functionalization strategy (figure 3(c)). An additional characteristic peak at 280 nm was attributed to the successful grafting of antibodies on E-rGO and this peak arises from the aromatic structures (tryptophan, phenyl alanine etc.) present in the antibody[12].

The X-ray diffraction (XRD) patterns of GO and E-rGO are shown in figure 3(d). The GO and E-rGO showed a broader (002) peak centered at around 12.2 and 25.7 degrees respectively. The XRD peak for the E-rGO was shifted to a high degree compared with the GO, indicating that the interlayer spacing of GO was larger than that of E-rGO. This could be attributed to the oxygen-containing groups but after electrochemical reduction abundant oxygen functional groups get diminished causing a decrease in d-spacing of E-rGO[39]. Raman spectra of the GO and electroreduced E-rGO was collected by exciting the sample with a 514 nm laser (figure 3(e)), which helped in understanding the type and intensity of the structural defects in the E-rGO nanostructures. A crystalline G band around 1580 cm^{-1} corresponds to vibrations of sp^2 rings in

View Article Online
DOI: 10.1039/C7TB01382E

the two-dimensional hexagonal lattice of Graphene, whereas the disordered D band around 1340 cm^{-1} attributed to the scattering caused by the defects produced in sp^2 hybridized termination plane of disordered carbonaceous material[40]. The relative I_D/I_G ratio of E-rGO and GO is 0.85 and 0.98 respectively, implying a crystalline nature and the presence of lower disorders and structural defects in the structure of the E-rGO as compare to GO. Also, the number of graphene layers can be depicted from the width and shape of 2D peak (~ 2672 cm^{-1}) which shows a decrease after reduction of E-rGO [41,42]. A broad and distinct Raman peak at around 2800–3000 cm^{-1} is also typical for the vibrations of proteins (figure (3f))[43]. The detail XPS analysis of E-rGO immobilized SPE and further insight deconvoluted peaks of C1s and O1s peaks are presented in figure 4. Peaks arised at ~ 288.5, ~ 287, ~ 285.8 eV are associated with oxygenated functional groups such as carboxyl, carbonyl, and hydroxide, respectively[39,44]. Peak centered at 284.5 eV is attributed to the non-oxygenated carbon lattice groups such as C=C, C–C, and C–H. The peaks originated at ~ 535 and ~ 533 and ~531 are assigned to the C-OH, C=O and O=C-OH respectively. These obtained results of XPS are also supported with EDS analysis.

The GO was spread over the surface of dual working electrodes of SPEs and electroreduced by the LSV technique. A potential reductive scan from 0 to -1.4 V was applied to check hydroxyl (-OH) or other oxygen containing moieties present in the parent GO molecules (represented in figure 5(a)). The appearance of a characteristic peak at −0.75 V indicative of the presence of detrimental oxygen moieties[25]. With increase in the number of reductive scans, the peak gets diminished leading to the formation of electro-reduced graphene free from any oxygen moiety and electroreduction of functional group (e.g., –OH, –COOH) on the surface of the GO. Further 10 cycles of CV (figure (5b)) were employed for the complete electrodeposition of E-rGO

View Article Online
DOI: 10.1039/C7TB01382E

nanosheets. CV electrochemical measurements at different steps of immunosensor development have been used to confirm the desired reduction, functionalization and antibody bioconjugation. The CV characteristics illustrated in figure 5(c) for the redox of ferro/ferri E-rGO modified electrodes exhibited manifold increase in anodic and cathodic peak current as compared to the bare SPE surface and GO. The graphene modification of the electrodes showed higher peak currents indicating a larger electro active area in comparison to bare SPE. This behavior is an indicative of a better electroactive nature of the E-rGO. The effective surface area of electrodes at different modification steps was calculated using the method described by Yola et al.[45,46].

$$ip = 2.69 \times 10^{5} n^{3/2} A D^{1/2} C v^{1/2} \quad \text{Equation (1)}$$

Where ip - peak current, A- electrode surface area, n- number of electrons transferred, D- diffusion coefficient, C- concentration of redox media, and v- scan rate. The estimated surface areas for the

GO immobilized SPE (GO/SPE), E-rGO immobilized SPE (E-rGO/SPE), and Antibody immobilized E-rGO/SPE (Ab@E-rGO/SPE) were 0.0273, 0.0345, and 0.0314 $cm^{2,}$ respectively. For electrochemical prospective, the graphene and its derivatives like E-rGO, have been shown to effectively increase the redox currents by contributing to the charge transfer and mass transfer processes. This is feasible due to its high porosity and interface surface area. Accordingly, the modification of the bare dual working SPEs with E-rGO led to a significant enhancement in the electrocatalytic activity of the electrode. The electrocatalytic activity of antibody immobilized E-rGO biointerface was also compared with antibody immobilized chemically reduced graphene oxide (C-rGO) biointerface and illustrated in figure S12, ESI. The antibody immobilized E-rGO shows better enhancement in the cathodic and anodic current and helps to amplify the signal

View Article Online
DOI: 10.1039/C7TB01382E

generated in comparison to the antibody immobilized C-rGO. The E-rGO has less defects on its 2D surface and free from contamination arising from the residue or excess toxic and hazardous reducing chemicals that exist in the solution phase chemistry used for the chemical reduction. In the electroreduction, the reduction of oxygen functionalities is achieved through a precise and controllable manner by simply adjusting the electrode potentials. The carboxyl groups remains intact for further antibody conjugation via carbodiimide chemistry. Whereas, in the chemical reduction method, the use of more than one reducing agents or steps may be required to achieve effective reduction of oxygen functionalities of the GO to the same extent, which could generate defects on the basal plane of sp^2 hybridized graphene sheets, and ultimately leading to less conduction behavior. In chemical reduction method, carboxyl functional groups (-COOH) present in GO also get reduced along with other hydroxyl, epoxy groups, which impedes the antibody loading and protein immobilization due to the unavailability of sufficient functional groups. Figure 5(d) presents the CV response over the ten cycles; the data indicates that the approach adopted for the preparation of the Graphene modified SPEs should allow the realization of stable and reproducible electrodes. The current intensity became constant and a stage is reached where electrochemically active surface area reached at its maximum value. Note that there was no mismatch in the redox peaks with satisfactorily stable current values. The interaction between the carbon SPEs and Graphene is strong enough to impart good stability, resulting from the well-known π–π and aromatization interactions.

The developed biointerface was studied for the quantification NEFA and βHBA biomarkers by using electrochemical label free technique such as DPV and chronoamperometric detection (AD).

View Article Online
DOI: 10.1039/C7TB01382E

Based on the well-known redox behavior of the E-rGO modified dual working SPEs in the ferro/ferri electrolyte buffer, the utility and performance of the Ab@E-rGO/SPE developed herein were demonstrated by using them for the quantification of their respective counter antigen, NEFA and βHBA, over a wide analyte concentration range (*i.e.* from 0 to 10 mM, in PBS buffer of pH 7.4); the results of the sensor output based on DPV are shown in figure 6(a) and 6(b) and their corresponding linear regression fit of current *vs.* analyte concentration are shown in figure 6(e) and 6(f), validated the linear range of analysis for NEFA from 0.1 mM to 5 mM ($R^2 \sim 0.99$, with a Detection Limit ~ 0.111 mM) and βHBA from 0.7 mM to 2 mM ($R^2 \sim$ 0.99, with a detection Limit 0.110 mM). The detection limit was determined according to the 3s/m criteria, where s represents the standard deviation of blank and m denotes the slope of the calibration plot. Such a wide concentration range highlights the potential applicability of this new E-rGO immunonosensor design in other biosensing applications as well as the results showed the remarkable enhancement and covered the wide range in comparison to the previous studies for the detection of NEFA and βHBA.[27,28,47,48] These results highlighted a decrease in the current with increasing antigen concentrations. In particular, the present system is able to detect the analyte over a very wide linear range. This decrease in the electrochemical response of the antibody-containing electrode is attributed to the non-conducting behavior of biomolecules. The peak current corresponding to the reduction of Fe^{3+} to Fe^{2+} decreased with an increase in NEFA and βHBA level due to the passivation of electrode surface that blocks the diffusion of the redox marker ions. This passivation is due to the presence of insulating layers formed by the NEFA and βHBA antibody-antigen complex. Graphene nanostructures amplify the electron transfer signals generated during the binding event of antibody and antigen as well as acting as a robust electrode material for protein immobilization with a high retention activity in electrochemical

View Article Online
DOI: 10.1039/C7TB01382E

reactions when used as a biosensor. Biosensing technology based on Graphene depends solely upon the amplification of signals generated by biological events resulting from biomolecules interfacing with these nanomaterials. When Graphene interacts with biomolecules, its electrical properties are modified – this change is the mechanism for the detection of a biological event. Graphene's electronic properties can also be influenced by the adsorption of molecules and atoms on its surface, and such surface modifications may also serve as local doping sites. The interaction of an analyte with Graphene should cause the introduction or withdrawal of electrons from its surface, which forms the basis for exploring this nanomaterial in the development of highly sensitive sensors. Moreover, the analysis of biomolecules by electrochemical immunosensors can be facilitated by an increase in the electrode's resistance due to the insulating nature of antibodies/antigens[49,50]. These results indicate that the fabricated E-rGO immobilized screen printed electrode exhibited a good analytical performance with standard samples, indicating its applicability for the investigation of other, real biological fluids. The practical utility of the Ab@E-rGO/SPE was then demonstrated by the analysis of NEFA and βHBA in some spiked Blood samples of healthy subjects and real clinical samples. Blood samples were spiked with known analyte concentrations (clinically significant levels) of NEFA and βHBA without any pretreatment or modification. The observed DPV response from different Ab@E-rGO SPEs was recorded with spiked blood, and the observed current values were correlated with the standard data and equations as shown in the calibration plots (figure 6(e) and 6(f)).

The values of the current as a function of the NEFA and βHBA concentration in standard samples are also estimated by the chronoamperometric technique (current *vs.* time) are plotted in

View Article Online
DOI: 10.1039/C7TB01382E

figure 6(c) and 6(d) and their corresponding linear regression fit of current *vs.* analyte concentration are plotted in figure 6(g) and 6(h). The Ab@E-rGO/SPE surface demonstrated a linear amperometric response with $R^2 \sim 0.99$. The detailed results of the electrochemical analysis of NEFA and βHBA by DPV are given in Table S1 and Table S2 respectively (ESI), which highlight that the immunosensing system proposed in this study was highly useful to reliably analyze the NEFA and βHBA concentrations in simulated serum samples and real clinical samples. Furthermore, the same DPV technique was utilized to analyze real clinical serum samples with unknown NEFA and βHBA concentrations (known concentrations were subsequently obtained from AHL, University of Guelph, Canada, where the precise βHBA and NEFA content was measured using a chemical analyser). Table S1 and S2 (ESI) also shows the DPV response from Ab@E-rGO SPE electrodes studied with clinical serum samples containing unknown concentrations of NEFA and βHBA. The concentrations were estimated by using the linear equation from the standard plot (figure 6(e) and 6(f)). As the NEFA and βHBA concentrations changed, a linear change was observed in the current value of the Ab@E-rGO/SPEs. Furthermore, the spiked blood samples of NEFA and βHBA were also checked using chronoamperometry and the obtained current value is shown in Table S3 and S4 respectively.

The specificity of the developed immunosensor was then evaluated (figure 7(a)) against some close structurally associated t non-specific interferents (concentration was fixed 1mM), such as D (+) glucose (Glu), L-ascorbic acid (AA), uric acid (UA) and lactic acid solution (LA). As the results show, the presence of the above analytes did not affect the obtained current values. This demonstrates that the Ab@E-rGO electrodes should be highly selective toward the target molecule, βHBA and NEFA. The anti-βHBA antibodies-modified E-rGO SPE surface only

View Article Online
DOI: 10.1039/C7TB01382E

exhibited a perturbation in current response toward the βHBA, and not the other studied interferents, by virtue of the well-known specificity of antibodies towards their counterpart antigens. The similar expected results were obtained for NEFA antibody modified E-rGO SPE. The reproducibility of the both Ab@E-rGO working electrodes were also investigated by examining the response of different batches toward a fixed analyte concentration (1 mM of NEFA and βHBA) (figure 7(b)). All of the different electrodes yielded a similar sensor response, proving that the proposed Ab@E-rGO/SPE sensor design has satisfactory reproducibility. Additionally, the stability of the Ab@E-rGO sensors was also assessed with respect to prolonged storage conditions. Ab@E-rGO/SPE sensors were stored under refrigeration (4 °C) when not in use. The electrodes were tested for their response against 1 mM βHBA and NEFA during periodic intervals up to 90 days. As shown in figure S13 (ESI), a constant sensor response was retained and no significant loss of signal was observed during 90 days of storage. Moreover, the obtained results for βHBA and NEFA determination are consistent with standard techniques such as the use of a chemical analyzer and a commercial colorimetric assay kit (Cayman Chemicals β-Hydroxybutyrate (ketone body), Cedarlane Labs, Burlington, ON, Canada) and NEFA Colorimetric Kit (My Biosource, USA). The colorimetric assay was performed on the standard as well as the clinical samples. A standard graph of absorbance *vs.* concentration of NEFA and βHBA were plotted and is shown in figure 7(c) and 7(d) respectively. The detailed results obtained using the colorimetric kit are tabulated in Table S5 and S6 (ESI). Additionally, Table S7 and S8 (ESI) shows a comparison of the results obtained by utilizing the three different techniques (chemical analyzer, colorimetric kit and electrochemical method), and the validated values are further compared in figure 7(e) and 7(f). The proposed simple electrochemical approach used in this study exhibited a quick sensing response (<1 min) without any sample

View Article Online
DOI: 10.1039/C7TB01382E

pretreatment. The obtained results from our proposed electrochemical technique demonstrate its utility in the accurate determination of βHBA and NEFA in clinical samples, being reproducible in the detection range, and the performance was validated by comparison with existing commercial techniques.

4. Conclusions

In this research, we have reported for the first time an anti-NEFA and anti-βHBA antibody immobilized E-rGO (Electro reduced graphene oxide) based simple, low cost and dual portable electrochemical immunosensor for the simultaneous detection of NEFA and βHBA antigen in standard as well as real clinical samples. We adopted a facile and green electrochemical approach for the exfoliation and in-situ reduction of graphene oxide (GO) nanostructures to E-rGO without the use of any harsh or toxic chemicals. The successful reduction of graphene oxide over SPEs has been attained by means of LSV and cyclic voltammetry. Various characterization techniques have been used to confirm and explore the properties of E-rGO. The electrodeposited E-rGO nanostructures were then successfully and conveniently bioconjugated with very specific anti-βHBA and anti-NEFA antibodies over the surface of E-rGO modified SPEs, *via* a well-known covalent chemistry using carbodiimide chemistry. This newly developed biointerface was then studied for its utility in the detection of a clinically important biomarkers of negative energy balance (NEB), NEFA and gold standard marker of sub-ketosis, βHBA over a very wide linear detection range. The obtained responses were demonstrated to be linear, specific, stable and

View Article Online
DOI: 10.1039/C7TB01382E

reproducible in electronic readout form. The developed sensor also showed promising results to analyze real clinical serum samples, and the obtained data was successfully validated with existing techniques such as chemical analyzer and commercial colorimetric kits. Our obtained results from user friendly electrochemical methods are well competitive with the existing complex and traditional techniques. The miniature size of graphene nanostructures based disposable sensor can assist the fabrication of portable hand held device for the on farm monitoring and field applications.

Acknowledgments

The authors sincerely thank Ms. Helen Kocmarek at the Animal Health Laboratory of the University of Guelph, Ontario, Canada for providing clinical samples collected from dairy farms in South West Ontario. The authors thank the Natural Sciences and Engineering Research Council of Canada (400705) and the Ontario Ministry of Agriculture, Food and Rural Affairs (298613) for funding this study. The authors declare no conflict of interest.

References

1 A. Vasilescu, G. Nunes, A. Hayat, U. Latif and J.-L. Marty, *Sensors (Basel, Switzerland)*, 2016, **16**, 1863.

2 M. Veerapandian, S. Neethirajan, G. F. Erf, Z. Peng, B. Tesche, K. Kleinermanns, W. Wei, H. Tang, C. S. Ozkan and U. Paik, *RSC Adv.*, 2015, **5**, 75015–75024.

3 S. K. Tuteja, P. Sabherwal, A. Deep, R. Rastogi, A. K. Paul and C. R. Suri, *ACS applied materials & interfaces*, 2014, **6**, 14767–71.

4 A. K. Geim and K. S. Novoselov, *Nature materials*, 2007, **6**, 183–91.

5 A. H. Castro Neto, N. M. R. Peres, K. S. Novoselov and A. K. Geim, *Reviews of Modern*

View Article Online
DOI: 10.1039/C7TB01382E

Physics, 2009, **81**, 109–162.

6 K. S. Novoselov, A. K. Geim, S. V. Morozov, D. Jiang, M. I. Katsnelson, I. V. Grigorieva, S. V. Dubonos and A. A. Firsov, *Nature*, 2005, **438**, 197–200.

7 C. Chen, S. Rosenblatt, K. I. Bolotin, W. Kalb, P. Kim, I. Kymissis, H. L. Stormer, T. F. Heinz and J. Hone, *Nature Nanotechnology*, 2009, **4**, 861–867.

8 M. Y. Han, B. Özyilmaz, Y. Zhang and P. Kim, *Physical Review Letters*, 2007, **98**, 206805.

9 C. Berger, *Science*, 2006, **312**, 1191–1196.

10 K. S. Novoselov, A. K. Geim, S. V Morozov, D. Jiang, Y. Zhang, S. V Dubonos, I. V Grigorieva and A. A. Firsov, *Science (New York, N.Y.)*, 2004, **306**, 666–9.

11 M. Pumera, *Chemical record (New York, N.Y.)*, 2009, **9**, 211–23.

12 S. K. Tuteja, R. Chen, M. Kukkar, C. K. Song, R. Mutreja, S. Singh, A. K. Paul, H. Lee, K.-H. Kim, A. Deep and C. R. Suri, *Biosensors and Bioelectronics*, 2016, **86**, 548–556.

13 S. K. Tuteja, M. Kukkar, C. R. Suri, A. K. Paul and A. Deep, *Biosensors and Bioelectronics*, 2015, **66**, 129-135.

14 T. Cassagneau and J. H. Fendler, *Advanced Materials*, 1998, **10**, 877–881.

15 P. Avouris, Z. Chen and V. Perebeinos, *Nature Nanotechnology*, 2007, **2**, 605–615.

16 F. Schedin, A. K. Geim, S. V. Morozov, E. W. Hill, P. Blake, M. I. Katsnelson and K. S. Novoselov, *Nature Materials*, 2007, **6**, 652–655.

17 J. S. Bunch, A. M. van der Zande, S. S. Verbridge, I. W. Frank, D. M. Tanenbaum, J. M. Parpia, H. G. Craighead and P. L. McEuen, *Science (New York, N.Y.)*, 2007, **315**, 490–3.

18 R. M. Westervelt, *Science (New York, N.Y.)*, 2008, **320**, 324–5.

19 W. Yang, K. R. Ratinac, S. P. Ringer, P. Thordarson, J. J. Gooding and F. Braet, *Angewandte Chemie (International ed. in English)*, 2010, **49**, 2114–38.

20 X. Wu, Y. Hu, J. Jin, N. Zhou, P. Wu, H. Zhang and C. Cai, *Analytical Chemistry*, 2010, **82**, 3588–3596.

21 Y. Shao, J. Wang, M. Engelhard, C. Wang and Y. Lin, *J. Mater. Chem.*, 2010, **20**, 743–748.

22 V. C. Tung, L.-M. Chen, M. J. Allen, J. K. Wassei, K. Nelson, R. B. Kaner and Y. Yang, *Nano letters*, 2009, **9**, 1949–55.

23 G. K. Dimitrakakis, E. Tylianakis and G. E. Froudakis, *Nano letters*, 2008, **8**, 3166–70.

View Article Online
DOI: 10.1039/C7TB01382E

24 S. K. Tuteja, Priyanka, V. Bhalla, A. Deep, A. K. Paul and C. R. Suri, *Analytica chimica acta*, 2014, **809**, 148–54.

25 P. Sharma, S. K. Tuteja, V. Bhalla, G. Shekhawat, V. P. Dravid and C. R. Suri, *Biosensors & bioelectronics*, 2013, **39**, 99–105.

26 L. Chen, Y. Tang, K. Wang, C. Liu and S. Luo, *Electrochemistry Communications*, 2011, **13**, 133–137.

27 X. Weng, L. Chen, S. Neethirajan and T. Duffield, *Biosensors and Bioelectronics*, 2015, **72**, 140–147.

28 M. Veerapandian, R. Hunter and S. Neethirajan, *Sensors and Actuators B: Chemical*, 2016, **228**, 180–184.

29 M. Iwersen, U. Falkenberg, R. Voigtsberger, D. Forderung and W. Heuwieser, *Journal of Dairy Science*, 2009, **92**, 2618–2624.

30 J. A. A. McArt, D. V. Nydam, P. A. Ospina and G. R. Oetzel, *Journal of Dairy Science*, 2011, **94**, 6011–6020.

31 P. A. Ospina, D. V. Nydam, T. Stokol and T. R. Overton, *Journal of Dairy Science*, 2010, **93**, 546–554.

32 M. Veerapandian, R. Hunter and S. Neethirajan, *Biosensors and Bioelectronics*, 2016, **78**, 253-258.

33 X. Weng, W. Zhao, S. Neethirajan and T. Duffield, *Journal of nanobiotechnology*, 2015, **13**, 13.

34 H. L. Guo, X. F. Wang, Q. Y. Qian, F. B. Wang and X. H. Xia, *ACS Nano*, 2009, **3**, 2653–2659.

35 A. Longo, R. Verucchi, L. Aversa, R. Tatti, A. Ambrosio, E. Orabona, U. Coscia, G. Carotenuto and P. Maddalena, *Nanotechnology*, 2017, **28**, 224002.

36 G. Wang, B. Wang, J. Park, Y. Wang, B. Sun and J. Yao, *Carbon*, 2009, **47**, 3242–3246.

37 B. Sun, Y. Gou, Y. Ma, X. Zheng, R. Bai, A. A. Ahmed Abdelmoaty and F. Hu, *Biosensors and Bioelectronics*, 2017, **88**, 55–62.

38 R. Su, S. F. Lin, D. Q. Chen and G. H. Chen, *The Journal of Physical Chemistry C*, 2014, **118**, 12520–12525.

39 K. Krishnamoorthy, M. Veerapandian, K. Yun and S.-J. Kim, *Carbon*, 2013, **53**, 38–49.

40 Konstantin N. Kudin, Bulent Ozbas, Hannes C. Schniepp, Robert K. Prud'homme, and

View Article Online
DOI: 10.1039/C7TB01382E

Ilhan A. Aksay and Roberto Car, *Nano letters*, 2008, **8**, 36–41.

41 C. Soldano, A. Mahmood and E. Dujardin, *Carbon*, 2010, **48**, 2127–2150.

42 I. K. Moon, J. Lee, R. S. Ruoff, H. Lee and P. E. Sheehan, *Nature Communications*, 2010, **1**, 1–6.

43 J. Surmacki, J. Musial, R. Kordek and H. Abramczyk, *Molecular cancer*, 2013, **12**, 48.

44 M. Koinuma, C. Ogata, Y. Kamei, K. Hatakeyama, H. Tateishi, Y. Watanabe, T. Taniguchi, K. Gezuhara, S. Hayami, A. Funatsu, M. Sakata, Y. Kuwahara, S. Kurihara and Y. Matsumoto, *The Journal of Physical Chemistry C*, 2012, **116**, 19822–19827.

45 M. L. Yola, T. Eren and N. Atar, *Electrochimica Acta*, 2014, **125**, 38–47.

46 J. Mehta, P. Vinayak, S. K. Tuteja, V. A. Chhabra, N. Bhardwaj, A. K. Paul, K. H. Kim and A. Deep, *Biosensors & bioelectronics*, 2016, **83**, 339–46.

47 M. Veerapandian, R. Hunter and S. Neethirajan, *Biosensors and Bioelectronics*, 2016, **78**, 253–258.

48 X. Weng, W. Zhao, S. Neethirajan and T. Duffield, *Journal of Nanobiotechnology*, 2015, **13**, 13.

49 S. Singh, S. K. Tuteja, D. Sillu, A. Deep and C. R. Suri, *Microchimica Acta*, 2016, **183**, 1729–1738.

50 S. Singh, N. Kumar, V. K. Meena, C. Kranz and S. Mishra, *Sensors and Actuators B: Chemical*, 2016, **237**, 318–328.

View Article Online
DOI: 10.1039/C7TB01382E

FIGURE CAPTIONS

Figure 1: Schematic illustration of the electrodeposition of Graphene nanostructures over the dual SPEs and by virtue of bioconjugation, the E-rGO (electro reduced graphene oxide) modified SPEs were then functionalized with NEFA and βHBA antibodies to develop a biointerface for Label free Electrochemical immunosensing. WE: working electrode.

Figure 2: (a) Bare working area of dual screen printed electrode (SPE) before electrodeposition; (b) Dual working electrode of SPE after electroreduction and electrodeposition of graphene nanostructures; (c) & (d) High magnification SEM images of electrodeposited E-rGO over the dual working area of SPEs ; (e) AFM image of E-rGO and (f) TEM image of E-rGO.

Figure 3: (a) FTIR analysis of GO and E-rGO; (b) UV-Vis study of GO and E-rGO; (c) UV- Vis spectrum of antibody conjugated E-rGO (Ab@E-rGO); (d) XRD analysis of GO and E-rGO; (e) Raman spectroscopic analysis of GO and E-rGO and (f) Raman spectrum of Ab@E-rGO.

Figure 4: XPS spectral study of E-rGO over the SPEs.

Figure 5: (a) LSV based electroreduction steps of GO to E-rGO; **(b)** Electrodeposition of MoS_2 by CV cycles; **(c)** the CV curves at different stages of SPE modification, recorded at a fixed scan rate of 50 mV s^{-1} in a redox probe solution of 10 mM $[Fe(CN)_6]^{3-}$ + 10 mM $[Fe(CN)_6]^{4-}$ prepared in 100 mM PBS buffer; **(d)** the cathodic current over 10 CV cycles.

Figure 6: (a) Representative DPVs of anti NEFA Ab@E-rGO SPE against various concentrations of antigen NEFA; (b) Representative DPVs of anti βHBA Ab@E-rGO SPE against various concentrations of antigen βHBA; (c) Chronoamperometric curve recorded from Ab@E-rGO SPE vs different concentrations of antigen NEFA; (d) Chronoamperometric curve recorded from Ab@E-rGO SPE vs different concentrations of antigen βHBA; (e) Calibration curve derived from DPVs of anti NEFA Ab@E-rGO SPE against various concentrations of

View Article Online
DOI: 10.1039/C7TB01382E

antigen NEFA; (f) Calibration curve derived from DPVs of anti βHBA Ab@E-rGO SPE against various concentrations of antigen βHBA; (g) Calibration curve derived from Chronoamperometric curve of NEFA; (h) Calibration curve derived from Chronoamperometric curve of βHBA.

Figure 7: (a) Investigations of sensor response towards NEFA and βHBA, in addition to other non-specific proteins to assess the device's specificity (concentration was fixed 1 mM), (b) reproducibility of the Ab@ErGO/SPEs and electrode to electrode variation by examining the response of different batches toward a fixed analyte concentration (1 mM); (c)&(d) Standard calibration plot using a commercial colorimetric kit of NEFA and βHBA respectively; (e) & (f) Comparison and validation of our developed electrochemical technique by the determination of NEFA and βHBA concentrations in clinical samples using 3 different techniques.

Figure 1

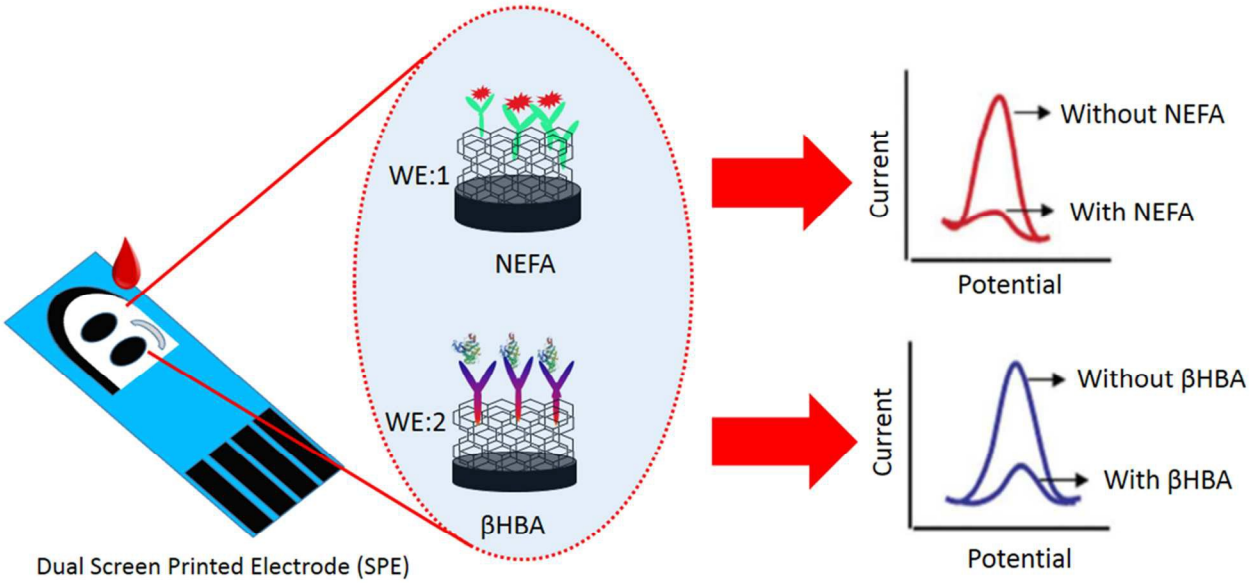

View Article Online
DOI: 10.1039/C7TB01382E

Figure 2

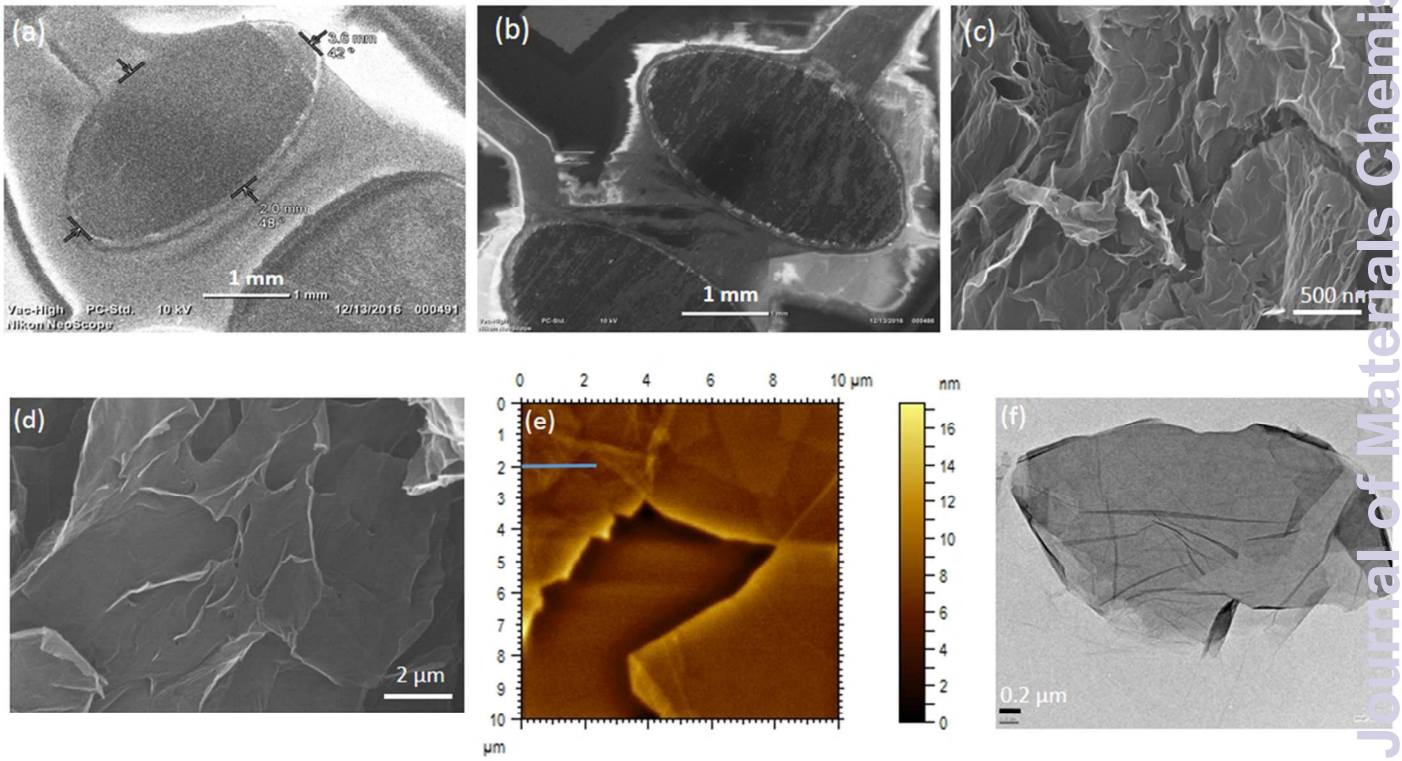

View Article Online
DOI: 10.1039/C7TB01382E

Figure 3

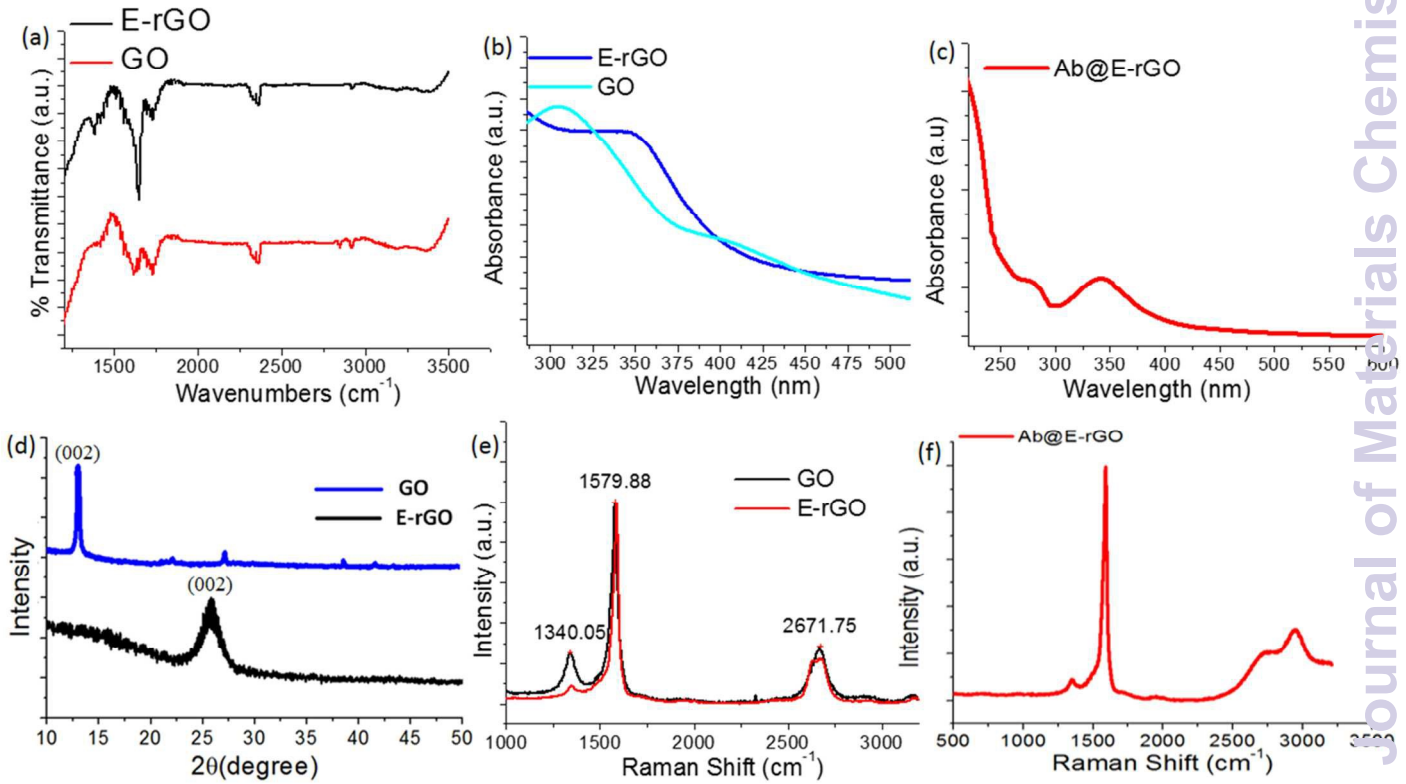

View Article Online
DOI: 10.1039/C7TB01382E

700

701

702

703

704

705

706

707

708

709

Figure 4

View Article Online
DOI: 10.1039/C7TB01382E

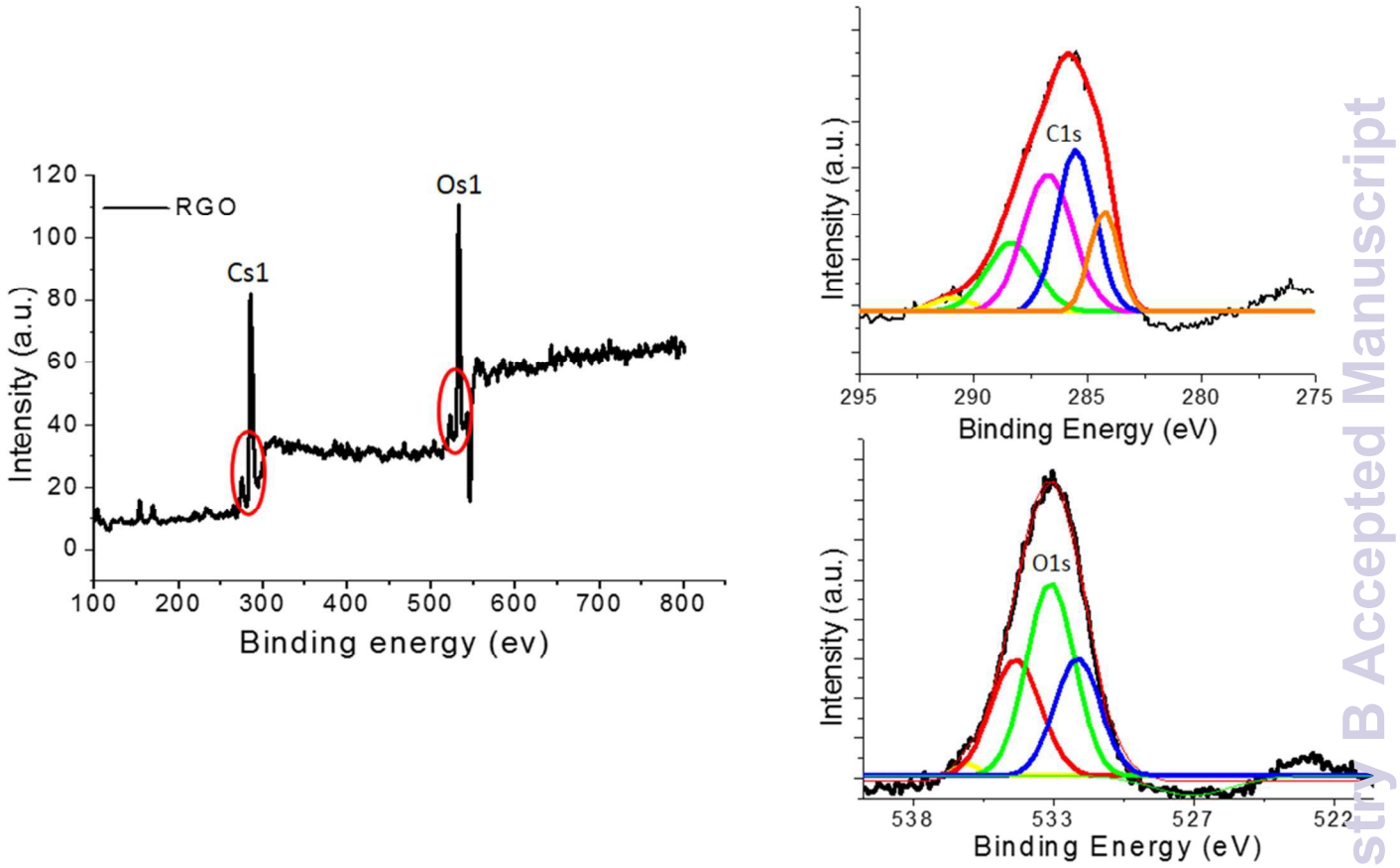

Figure 5

View Article Online
DOI: 10.1039/C7TB01382E

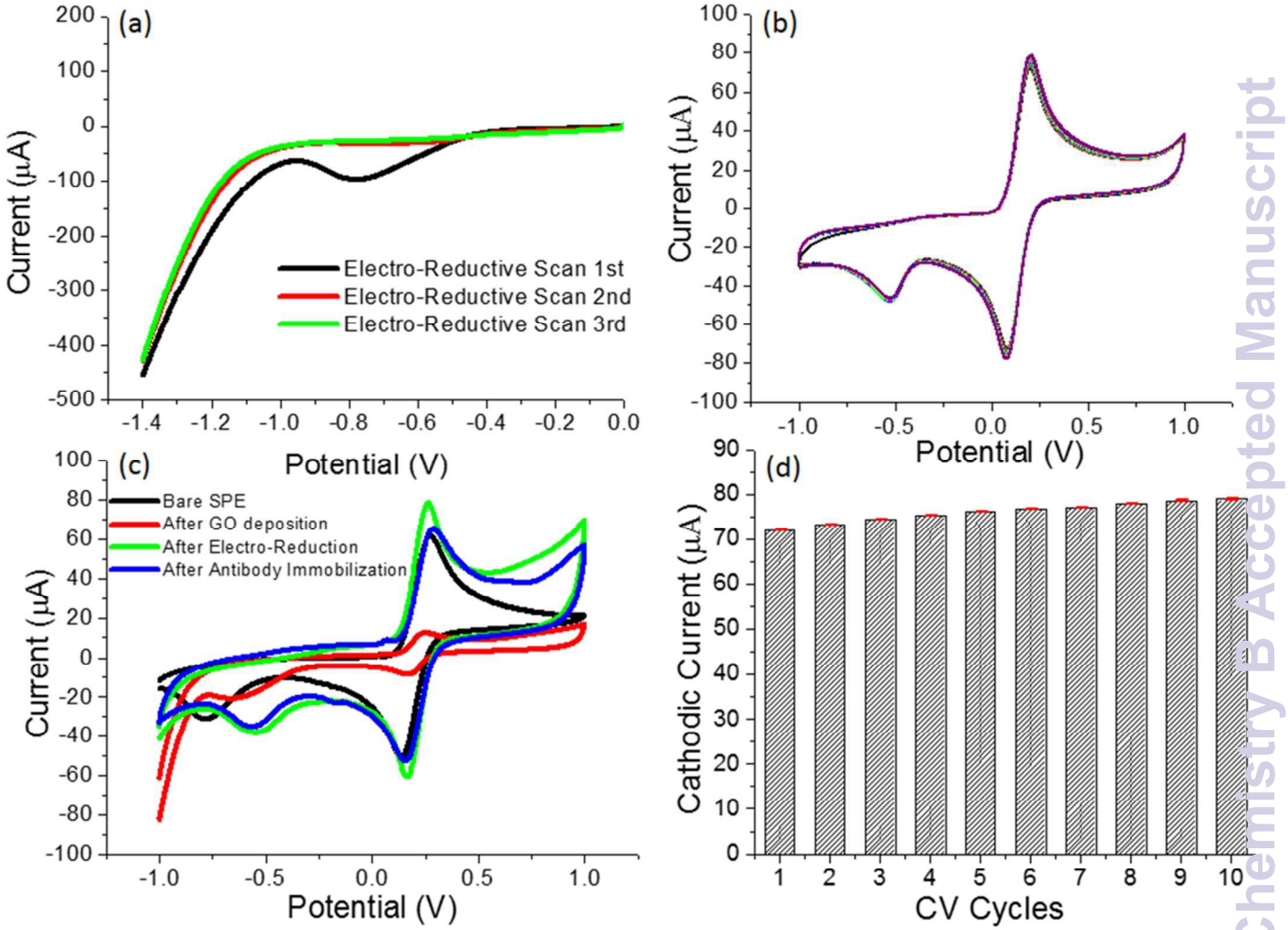

Figure 6

View Article Online
DOI: 10.1039/C7TB01382E

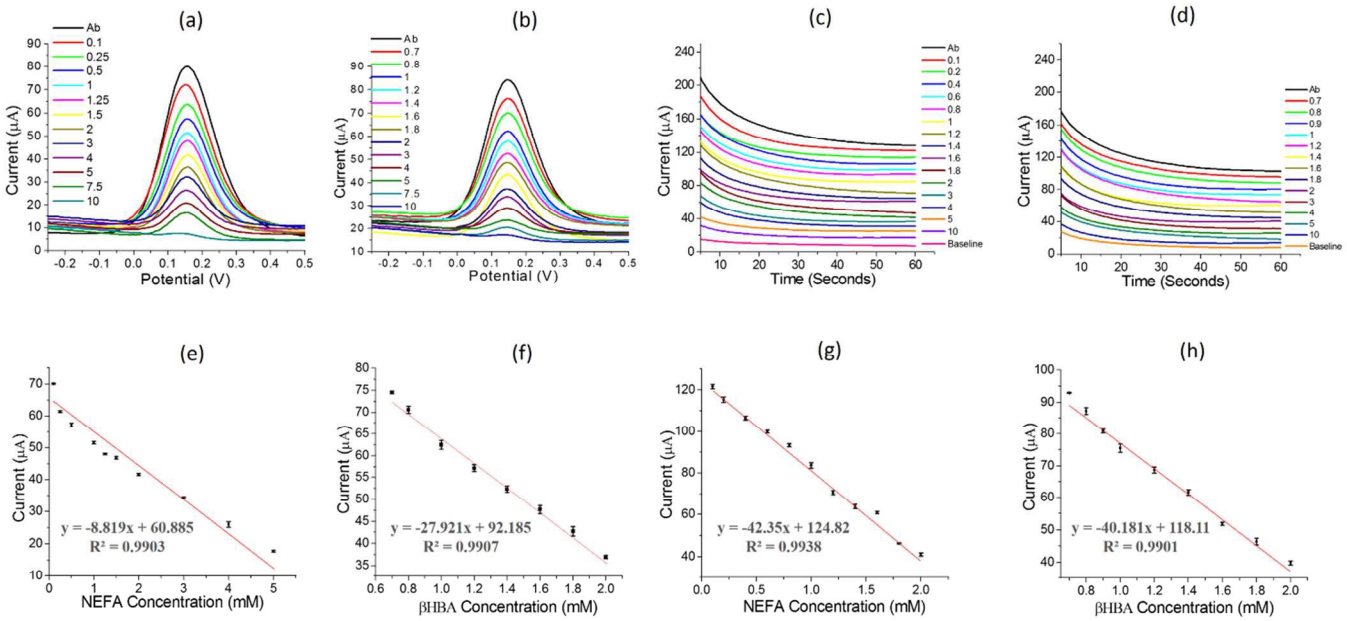

Figure 7

View Article Online
DOI: 10.1039/C7TB01382E

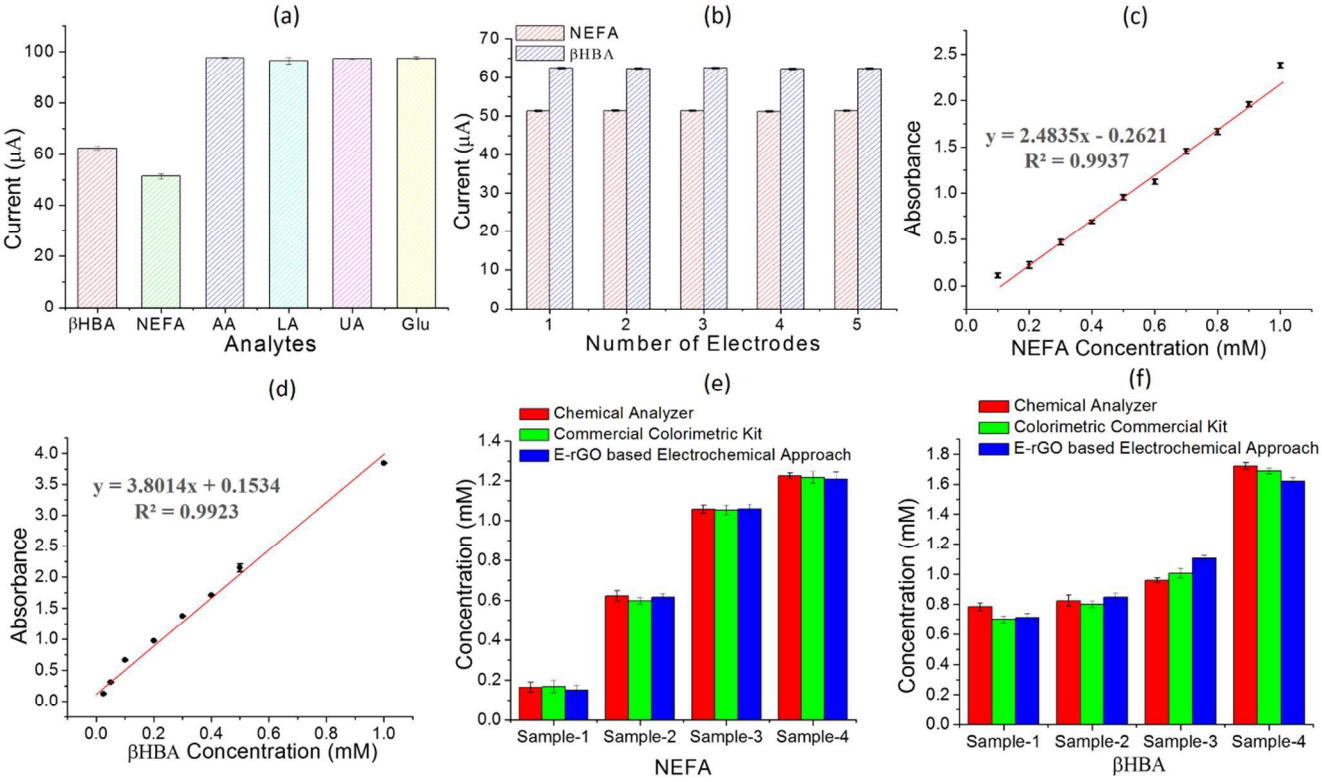

742

View Article Online
DOI: 10.1039/C7TB01382E

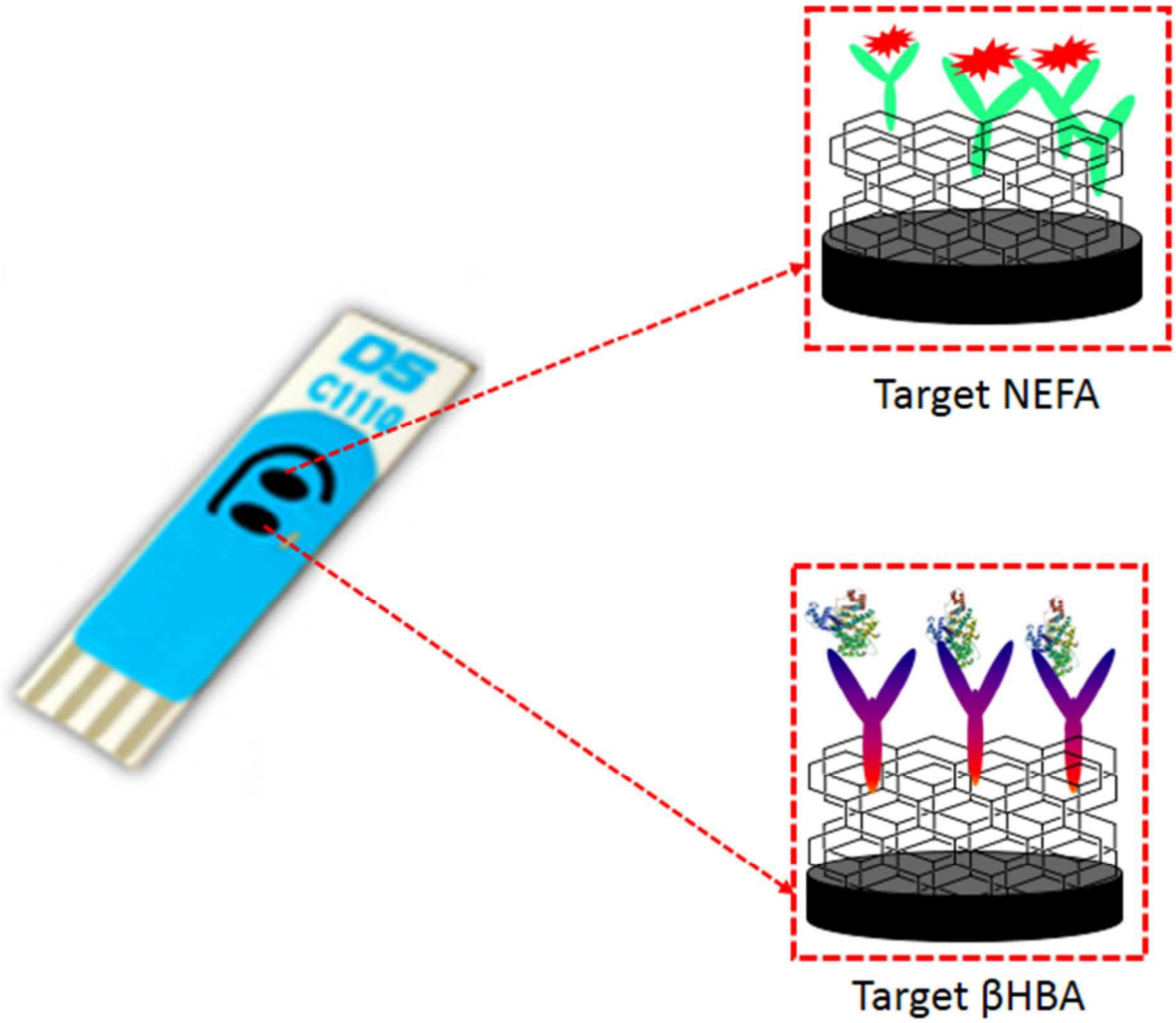

Label-free assay using electrodeposited antibody-conjugated graphene biointerface for dual detection of NEFA and βHBA from dairy cow blood samples